Amorphous Mixtures of Ice and C_{60} Fullerene

*Siriney O. Halukeerthi,[a] Jacob J. Shephard,[a,b] Sukhpreet K. Talewar,[a] John S. O. Evans,[b] Alexander Rosu-Finsen,[a] Christoph G. Salzmann[a]**

[a] Department of Chemistry, University College London, 20 Gordon Street, London WC1H 0AJ, United Kingdom; e–mail: c.salzmann@ucl.ac.uk

[b] Department of Chemistry, Durham University, South Road, Durham DH1 3LE, United Kingdom

Table of Contents

1. Composition of C_{60} / H_2O samples

Different molar ratios of H_2O and C_{60} in the C_{60} / H_2O samples were obtained by adjusting the deposition rates of H_2O and C_{60}.

1.1 Constant H_2O flow with varying amounts of C_{60}

Firstly, the deposition of H_2O at 85 K was monitored with a quartz crystal microbalance (QCM). The deposition rate of H_2O at an inlet pressure of 1.00×10^{-1} mbar was determined to be 0.85 µg cm^{-2} s^{-1} by performing a linear fit to the data shown in Fig. S1, where the gradient is equal to the mass deposition rate. This deposition rate was divided by the molar mass of H_2O (18.02 g mol^{-1}) to give a molar deposition rate of 4.75×10^{-2} µmol cm^{-2} s^{-1}.

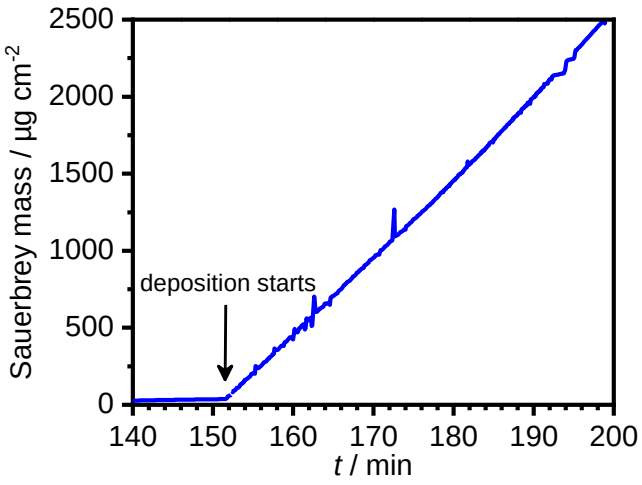

Fig. S1. Sauerbrey mass recorded during the deposition of pure H_2O at an H_2O inlet pressure of 0.100 mbar.

In the next step, the QCM response was recorded as C_{60} sublimed onto the deposition plate. For this, the temperature of the deposition source was set to a range of different temperatures. Once a specific temperature was reached, the pneumatic shutter above the crucible was lifted, allowing the C_{60} to be deposited onto the deposition plate. The shutter was then closed, and the temperature increased to the next desired temperature, as shown in Fig. S2(a). The deposition rate was then calculated by determining the gradients from the QCM data. In Fig. S2(b), the deposition rate of C_{60} is plotted against the temperature of the deposition source.

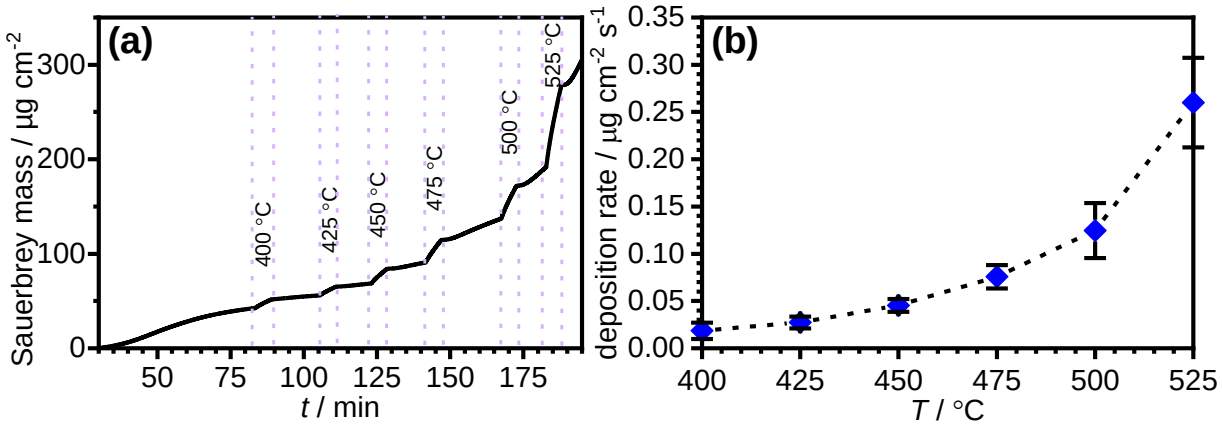

Fig. S2. (a) QCM response during a typical C_{60} calibration experiment. (b) The average mass deposition rate of C_{60} against the corresponding deposition source temperature.

The mass deposition rates of C_{60} at different deposition source temperatures were divided by the molar mass of C_{60} (720.66 g mol^{-1}) to obtain molar deposition rates as shown in Table S1.

Table S1: Average mass and molar deposition rates as well as H_2O:C_{60} molar ratios for each temperature of the deposition source and a water deposition rate of 4.75 × 10^{-2} µmol cm^{-2} s^{-1}.

T / °C	average C_{60} deposition rate / µg cm^{-2} s^{-1}	average C_{60} molar deposition rate / µmol cm^{-2} s^{-1}	H_2O:C_{60} molar ratio
400	1.86×10^{-2}	2.58×10^{-5}	1841:1
425	2.73×10^{-2}	3.79×10^{-5}	1254:1
450	4.54×10^{-2}	6.31×10^{-5}	754:1
475	7.57×10^{-2}	1.05×10^{-4}	452:1
500	1.25×10^{-1}	1.74×10^{-4}	274:1
525	2.60×10^{-1}	3.61×10^{-4}	132:1

In order to determine the molar ratios of the H_2O:C_{60} mixtures for a specific deposition source temperature, the molar deposition rate of H_2O was divided by that of C_{60}. The ratios and their errors are shown in Fig. S3.

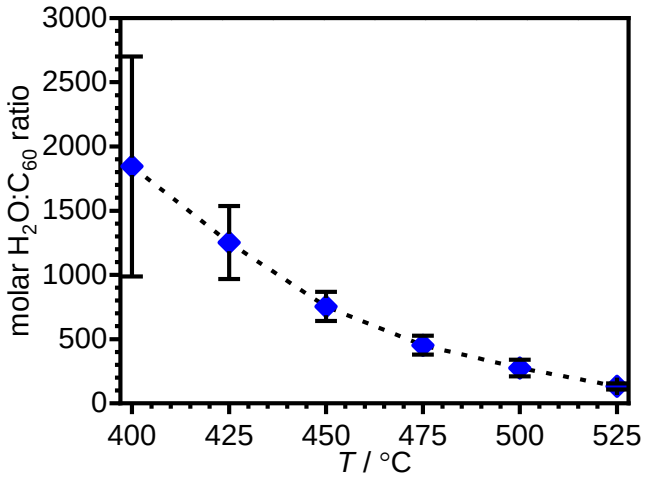

Fig. S3: Molar H_2O:C_{60} ratios as a function of the temperature of the deposition source and a water deposition rate of 4.75 × 10^{-2} µmol cm^{-2} s^{-1}. The relatively large error bar at 400°C is due to the low sublimation rate of C_{60}.

To realise a range of molar H_2O:C_{60} ratios and considering the errors, the chosen ratios were 1254:1 (source T = 425°C), 452:1 (T = 475°C) and 132:1 (T = 525°C).

1.2 Varying the H_2O flow with constant amounts of C_{60}

In section 1.1, the H_2O inlet pressure was set to 1.00 × 10^{-1} mbar, which resulted in a deposition rate of 0.85 µg cm^{-2} s^{-1}. To extend the composition range towards more C_{60}-rich mixtures, the H_2O inlet pressure was reduced in the following while the deposition source was maintained at 525°C.

The first step for calculating the ratios was to determine the deposition rates of H_2O for inlet pressures of 5.00 × 10^{-3} mbar, 2.00 × 10^{-2} and 5.00 × 10^{-2}, using the QCM as shown in Fig S4.

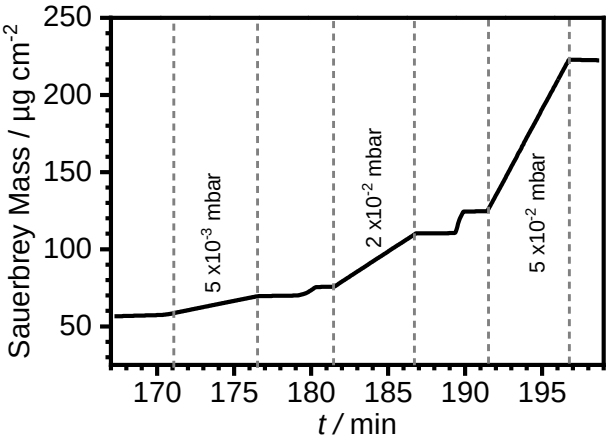

Fig. S4: QCM response during the H_2O calibration experiment by varying the inlet pressure.

As shown in Table S2, the deposition rates were divided by the molar mass of H_2O to obtain molar deposition rates.

Table S2: H_2O inlet pressures with their corresponding mass and molar deposition rates as well as H_2O:C_{60} molar ratios with 3.61 × 10^{-4} µmol cm^{-2} s^{-1} C_{60}.

inlet pressure / mbar	deposition rate / µg cm^{-2} s^{-1}	molar deposition rate / µmol cm^{-2} s^{-1}	H_2O:C_{60} molar ratio
5.00×10^{-2}	0.31	1.72×10^{-2}	48:1
2.00×10^{-2}	0.11	6.02×10^{-3}	17:1
5.00×10^{-3}	0.03	1.87×10^{-3}	5:1

The molar deposition rate values were then divided by the deposition rate of C_{60} at 525°C (3.61 × 10^{-4} µmol cm^{-2} s^{-1}) to determine the H_2O:C_{60} ratio of mixtures at the different H_2O inlet pressures as shown in Fig. S5.

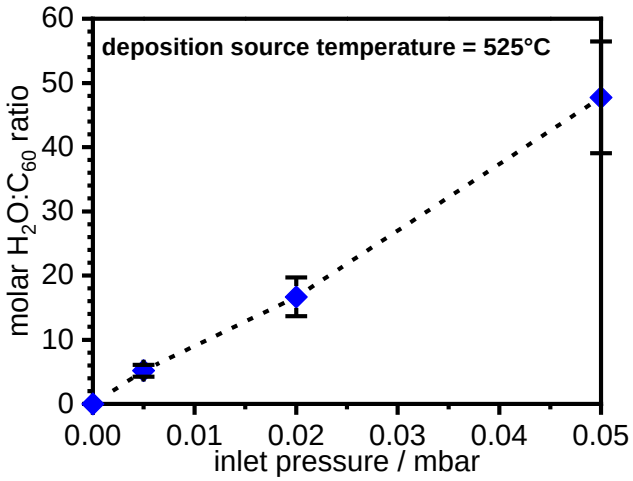

Fig. S5: Molar H_2O:C_{60} ratios at a constant deposition source temperature of 525 °C and varying the H_2O inlet pressures.

1.3 Molecular-volume percentages of C_{60} in C_{60} / H_2O mixtures

First, the molar volume of low-density amorphous ice (LDA) was calculated. The density of LDA is known to be 0.93 g cm^{-3}, therefore the density can be divided by the molar mass of H_2O to give a molar volume of 5.16×10^{-2} mol cm^{-3}. The molecular volume was calculated as 3.21×10^{-23} cm^3 or 32.18 $Å^3$.

The second step was to determine the molar density of C_{60} at cryogenic temperatures. From the cubic lattice constant a = 14.05 Å at 80 K, the density of C_{60} was calculated to be 1.74 g cm^{-3}.[1-2] The molecular volume of C_{60} was therefore determined to be 687.77 $Å^3$.

In Table S3, the molecular volumes of LDA and C_{60} were used to work out the molecular volume percentages of C_{60} for the various mixtures. These calculations assume a zero excess volume.

Table S3: C_{60}:H_2O molar ratios with their corresponding C_{60} molecular-volume percentages.

T / ℃	C_{60}:H_2O molar ratios	C_{60} volume percent / %
425	1:1254	1.7
475	1:452	4.5
525	1:132	14
525	1:48	31
525	1:17	56
525	1:5	81

2. Additional X-ray diffraction patterns

2.1 Comparison with the XRD pattern of bulk C_{60}

The XRD patterns of bulk C_{60} at room temperature and the most C_{60}-rich sample (1:17) at –3°C are shown in Figure S6. The pattern of bulk C_{60} agrees well with those reported in the literature.[1]

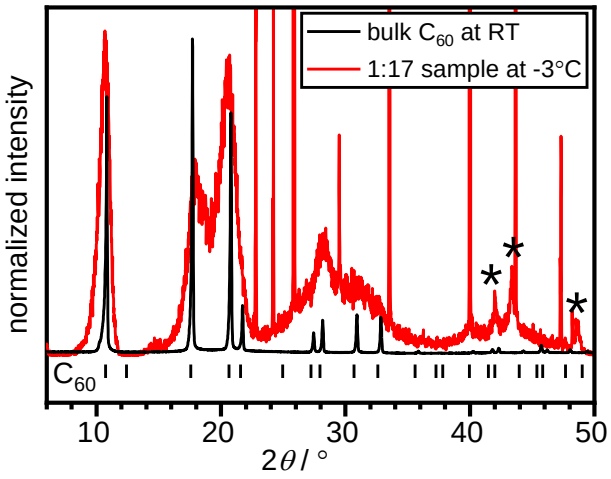

Fig. S6: Comparison of the XRD patterns of bulk C_{60} at room temperature and the most C_{60}-rich sample (1:17) at –3°C (λ= 1.54 Å). The sharp Bragg peaks of the 1:17 sample arise from ice Ih. Features marked with asterisks originate from the sample holder.

2.2 X-ray diffraction patterns of C_{60} / H_2O mixtures heated from 95 K to 270 K

Complete set of XRD artificial heat maps of the pure H_2O and the C_{60}/H_2O mixtures ranging from 1.67 - 56.03 v% C_{60} is shown in Fig. S7. XRD data of the 80.44 v% C_{60} sample could not be collected due to the finely powdered nature of the sample.

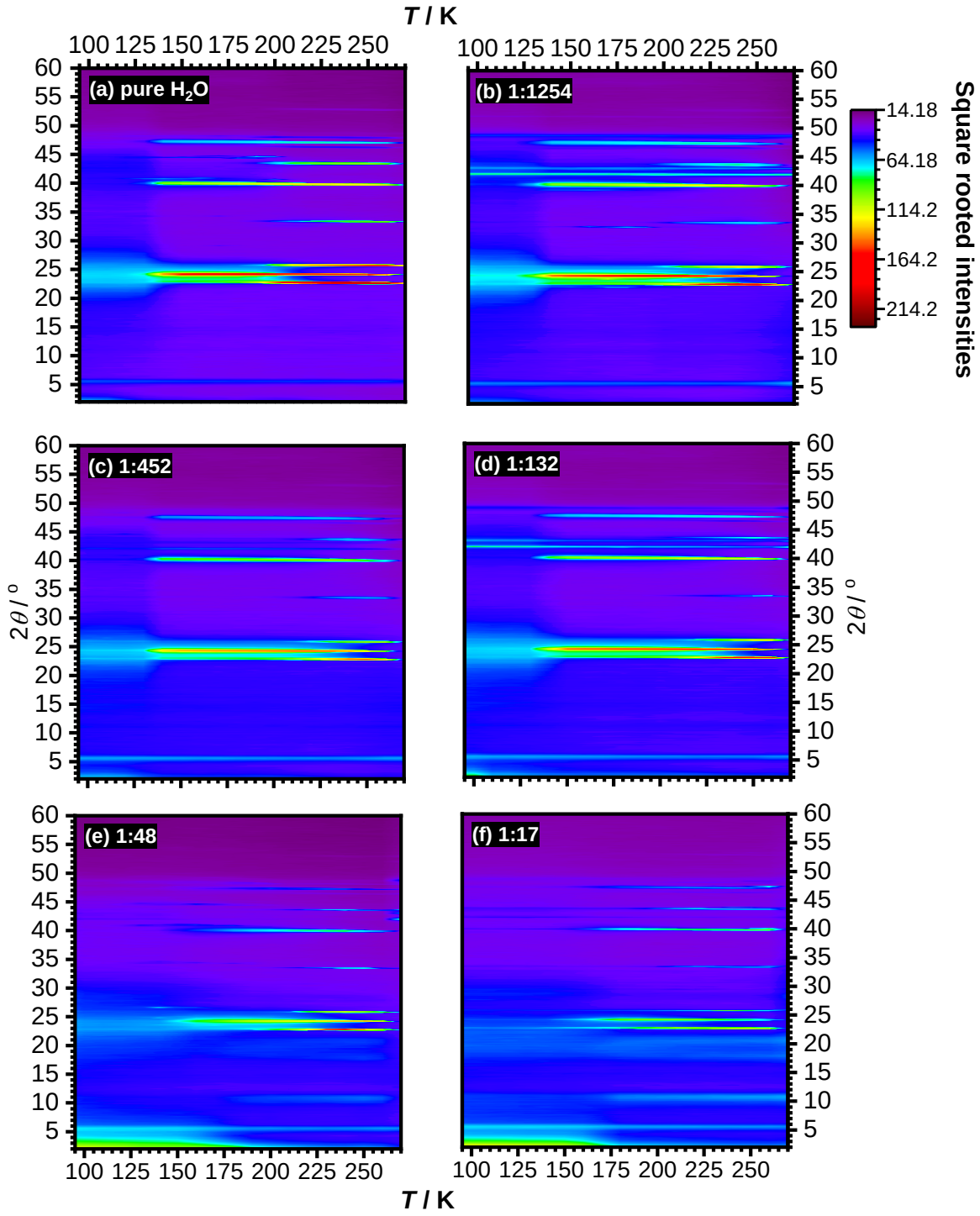

Fig. S7. Contour plots of X-ray diffraction patterns (λ= 1.54 Å) recorded upon heating at ambient pressure of pure H_2O and C_{60}:H_2O mixtures with the indicated molar ratios.

2.3 MCDIFFaX fits of the 150 K diffraction patterns

Detailed background information on stacking disorder in ice and the MCDIFFaX approach are given in refs 3-5.

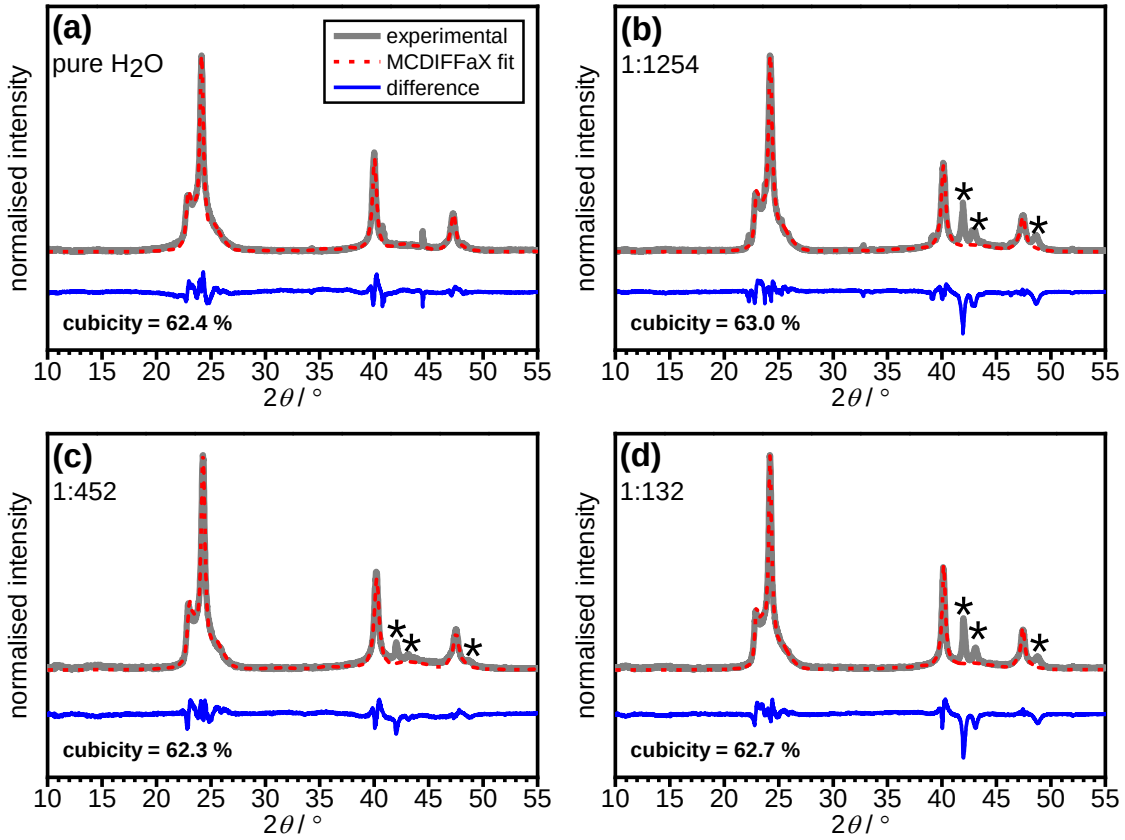

Fig. S8. MCDIFFaX fits of the XRD patterns (Cu Kα) of ice Isd obtained after crystallizing (a) pure ASW and (b-c) C_{60} / H_2O mixtures at 150 K with the indicated C_{60}:H_2O molar rations. The obtained cubicities are noted for each sample. Features marked with asterisks are due to the brass sample holder.

2.4 Intensity of the (110) Bragg peak of ice I as a function of the cubicity

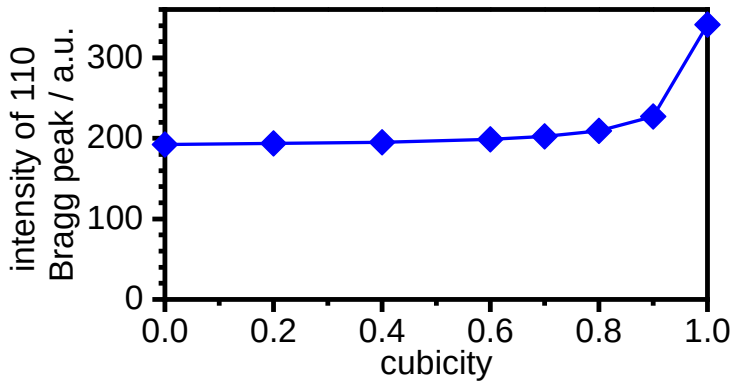

Fig. S9: Intensity of the (110) Bragg peak of ice I calculated with MCDIFFaX as a function of the cubicity.

3. SEM picture of a pure C_{60} film deposited at 90 K

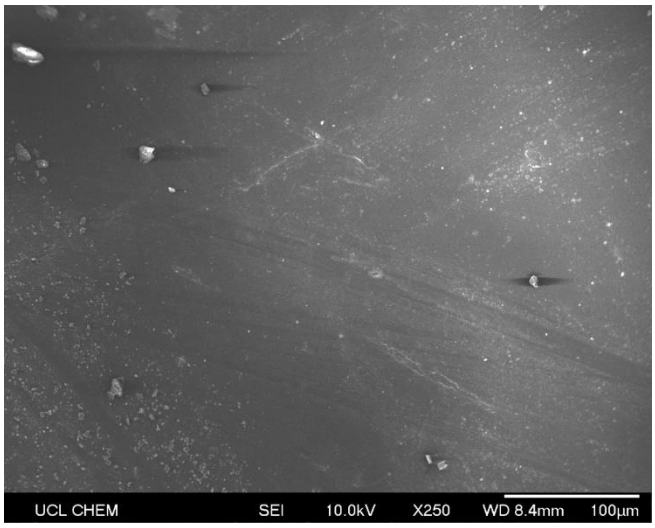

Fig. S10. SEM image of pure C_{60} on an aluminium SEM stub at 100 µm magnification.

4. References

1. Heiney, P. A.; Fischer, J. E.; McGhie, A. R.; Romanow, W. J.; Denenstein, A. M.; McCauley Jr, J. P.; Smith, A. B.; Cox, D. E., Orientational Ordering Transition in Solid C_{60}. *Phys. Rev. Lett.* **1991**, *66*, 2911-2914.
2. David, W. I. F.; Ibberson, R. M.; Dennis, T. J. S.; Hare, J. P.; Prassides, K., Structural Phase Transitions in the Fullerene C 60. *EPL* **1992**, *18*, 219-225.
3. Malkin, T. L.; Murray, B. J.; Brukhno, A. V.; J., A.; Salzmann, C. G., Structure of Ice Crystallized from Supercooled Water. *Proc. Natl. Acad. Sci. USA* **2012**, *109*, 1041-1045.
4. Malkin, T. L.; Murray, B. J.; Salzmann, C. G.; Molinero, V.; Pickering, S. J.; Whale, T. F., Stacking Disorder in Ice I. *Phys. Chem. Chem. Phys.* **2015**, *17*, 60-76.
5. Salzmann, C. G.; Murray, B. J.; Shephard, J. J., Extent of Stacking Disorder in Diamond. *Diam. Relat. Mater.* **2015**, *59*, 69-72.